The final publication is available at

https://doi.org/10.1016/j.carbon.2012.02.050

Additional Information

# Carbon nanohorns functionalized with polyamidoamine dendrimers as efficient biocarrier materials for gene therapy

*Javier Guerra* [a,b], *M. Antonia Herrero* [a], *Blanca Carrión* [b], *Francisco C. Pérez-Martínez* [b], *Maribel Lucío* [a], *Noelia Rubio* [a], *Moreno Meneghetti* [c], *Maurizio Prato* [d], *Valentín Ceña* [b,e], *Ester Vázquez* [a,*]

[a] *Departamento de Química Orgánica, Facultad de Químicas-IRICA, Universidad de Castilla-La Mancha, Campus Universitario, 13071 Ciudad Real, Spain*

[b] *NanoDrugs, S.L., Paseo de la Innovación 1, Campus Universitario, 02006 Albacete, Spain*

[c] *Dipartimento di Scienze Chimiche, Università di Padova, Via Marzolo 1, 35131 Padova, Italy*

[d] *Center of Excellence for Nanostructured Materials (CENMAT) & Italian Interuniversity Consortium on Materials Science and Technology(INSTM – Unit of Trieste), Dipartimento di Scienze Farmaceutiche, Università degli Studi di Trieste, Piazzale Europa 1, 34127 Trieste, Italy* [e] *Unidad Asociada Neurodeath, Farmacología, CSIC-Universidad de Castilla-La Mancha, Campus Universitario, 02006 Albacete, Spain*

## ABSTRACT

Carbon nanohorns are suitable platforms for use in biological applications. Their high surface areas allow the incorporation of molecular entities, such as polyamidoamine dendrimers. In this work, we report the synthesis, structural characterization and biological data of new hybrid systems of carbon nanohorns that hold polyamidoamine dendrimers. One of these derivatives has been employed as an agent for gene delivery. The system is able to release interfering genetic material diminishing the levels of a house-keeping protein and a protein directly involved in prostate cancer development. Importantly, this hybrid material is also far less toxic than the corresponding free dendrimer. These results allow us to conclude that these nanomaterials can be exploited as useful non-viral agents for gene therapy.

## 1. Introduction

Carbon nanohorns (CNHs) represent a new type of carbon nanomaterial. CNHs consist of single graphene tubes of 2–5 nm in diameter and a length around 40–50 nm, with a conically-closed tip. CNHs usually aggregate in assemblies that are reminiscent of dahlia flowers with a diameter that goes from 80 to 100 nm, although they can also form buds and seeds [1]. The use of CNHs in biological applications generates a series of advantages with respect to other carbon nanomaterials. Firstly, CNHs are synthesized in the absence of metal catalysts and with a high purity degree. Secondly, their size allows the inclusion of CNHs through endocytosis into the inner cell decreasing cytotoxicity [2–4]. Hence, these materials have already been used as carriers in nanomedicine. *Cis*-platin [5,6], doxorubicine [7] and dexametasone [8], two anticancer agents and an anti-inflammatory drug, respectively, have been linked to the CNH structure with promising results. Moreover, magnetite particles have also been included in the CNH structure aiming at the synthesis of targeted drug systems [9]. These contributions demonstrate that CNHs are suitable platforms for delivery purposes. Functionalization of the CNH structures

* *Corresponding author:* Fax: +34 926295318.

E-mail address: Ester.vazquez@uclm.es (E. Vázquez).

has also been useful broadening their applications and enhancing their solubility in aqueous media [10–12].

In previous works, we and others have demonstrated the potential of carbon nanomaterials for biological applications [13–15]. Different functionalized multi-walled carbon nanotubes (MWCNTs) have already shown potential advantage for the intracellular delivery of therapeutic agents, showing no toxicity *in vivo* [16–19] and recently polyamidoamine (PAMAM) dendron fragments attached to carbon nanotube surfaces have proved to be efficient non-viral agents for gene transfer [20,21]. Precisely tailored amino groups introduced as different dendron generations onto the multi-walled carbon nanotube surface have shown to be able to complex and effectively deliver double-stranded small interfering ribonucleic acid (siRNA) achieving gene silencing *in vitro*. A systematic comparison between different PAMAM dendron-functionalized MWCNT series in terms of cellular uptake, cytotoxicity, and siRNA complexation has recently been published [22].

In this paper we describe a new hybrid system based on PAMAM dendrimers anchored to the CNH surface. We have explored gene delivery as the biological application, because CNHs can be considered as ideal carriers to anchor biologically active molecules. In terms of gene delivery, on the one hand, PAMAM dendrimers will be responsible for the electrostatic binding to siRNA and they will also enhance the solubility of CNHs avoiding their aggregation. On the other hand, CNHs will serve as platform for dendrimers. CNHs possess a spherical shape and larger diameters than carbon nanotubes, which could lead to differences in the mechanism of metabolism, degradation or dissolution, clearance and bioaccumulation [15]. It is very likely that CNH [23] derivatives and free PAMAM dendrimers [24,25] share common features with respect to their biological role as carriers. Both systems are endocytocized within the cell, are incorporated into endosomes and finally, release the genetic material in the cytoplasm. However, these two systems have important dissimilarities. Surface charge density is clearly different in both structures. While in the unaltered PAMAM dendrimer, high surface charge density is inherent to its cationic polyamine surface, the elevated surface area that CNHs display allows an overall well-dispersed positive charge distributed along the carbon nanostructure. Surface charge density has previously been addressed as a cause for the high toxicity that amino-terminated PAMAM dendrimers display [26]. Moreover, the rigid location of the PAMAM dendrimers on the CNH surface inhibits dendrimer aggregation, which may protect the system from immunogenic responses [27]. One important fact that justifies the synthesis of this new hybrid material is that it is far less toxic than the corresponding free dendrimer. We attribute this distinctive feature to the different structure of both systems as aforementioned. Finally, the CNH structure permits further modifications for more rational design of transfection reagents to improve transfection efficiency in different cell types. In this work we also take advantage of the ability of PAMAM dendrimers to incorporate gold nanoparticles in their cavities [28]. Herein, we use these metallic particles as markers to determine the localization of the dendrimers along the surface of the carbon nanohorns.

## 2. Experimental section

### 2.1. Chemicals

G4-NH$_2$ and G6-NH$_2$ PAMAM dendrimers were purchased as a 10 and 5 wt.% methanol solution, respectively (Dendritech, Inc., Midland, MI). The methanol was removed under vacuum prior to use, and 18 MO cm Milli-Q deionized water (Millipore) was added to obtain aqueous solutions of G4-NH$_2$ and G6-NH$_2$ having the desired concentrations. HAuCl$_4$, NaBH$_4$ (99.9%, Reagent Plus), Boc-protected *p*-aminomethylaniline, isoamyl nitrite, methyl acrylate, *N*-ethyldiisopropylamine, HCl gas and methanol (Sigma–Aldrich, Inc.) were used as received. CNHs were produced by Carbonium s.r.l., Padova (Italy) by direct graphite evaporation in Ar flow, according to a patented method [29,30] and used without purification.

All experiments were carried out in air unless specified otherwise.

### 2.2. Characterization

Transmission electron microscopy (TEM) experiments were performed using a FEI Tecnai G2 F20 transmission electron microscope, equipped with Schottky-type field emission gun, X-twin lenses, an EDAX energy-dispersive X-ray spec- trometer (EDS), and a scanning TEM (STEM) unit with high- angle annular dark-field (HAADF) detector operating at 200 kV (The University of Texas at Austin) or using a Philips EM 208, accelerating voltage of 100 kV (University of Trieste). Samples were prepared by sonication for 10 min and drop- wise (8 1L) addition of the sample onto a carbon coated 400 mesh Cu grid (EM Sciences, Gibbstown, NJ) followed by sol- vent evaporation in air.

Thermogravimetric analyses (TGA) were obtained using a TGA Q50 (TA Instruments) and recorded under N$_2$ or under an air atmosphere by equilibrating at 100 °C followed by a ramp of 10 °C/min up to 1000 °C.

The hydrodynamic diameter of the particles was determined using a dynamic light scattering (DLS, ZetaPlus, Brookhaven, Holtsville, NY) instrument operating at a 90° scattering angle with a 635 nm, 35 mW diode laser source. 0.5 mL of functionalized carbon nanohorns (8.3 1g/mL) at pH = 5.35 as well as incubated with 33.3 nM of siRNA were used for these studies. The path length of the cuvette was 1 cm. Each sample was run ten times and each run lasting 5 min at 298 K. The data were fitted using the non-negatively constrained least squares (NNLS) algorithm [31] to solve the experimentally measured autocorrelation function.

### 2.3. Synthesis of the different CNH derivatives

#### 2.3.1. Synthesis of functionalized CNHs (see Fig. 1)
*2.3.1.1. Boc-protected CNH intermediate.* In a typical experiment, 40 mg of pristine CNHs were sonicated in deionized water together with Boc-protected *p*-aminomethylaniline(1.53 g, 6.92 mmol) for 10 min in a microwave glass vessel. Finally, isoamyl nitrite (0.44 mL, 3.34 mmol) was added, and a condenser was placed. The mixture was irradiated at 80 °C working at 100 W for 30 min, and after addition of a new

aliquot of isoamyl nitrite (0.44 mL, 3.34 mmol), at 30 W for 60 min. After cooling at room temperature, the crude was filtered on a Millipore membrane (GTTP, 0.2 1m). The collected black solid was washed using cycles of sonication and filtration with methanol until the filtrate was clear and finally dried under high vacuum affording 36 mg of Boc-protected CNH intermediate.

*2.3.1.2. f-CNH1.* HCl gas was bubbled for 5 min through a suspension of Boc-protected CNH intermediate (34.5 mg) in methanol (30 mL). The reaction mixture was stirred at room temperature for 14 h, filtered on a Millipore membrane (GTTP, 0.2 1m) and washed by cycles of sonication and filtration using 75 mL of a mixture water/methanol (1:1). The collected black solid was finally dried under high vacuum affording 34.5 mg of *f*-CNH1.

*2.3.1.3. f-CNH2.* Twenty milligrams of *f*-CNH1 were sonicated in methanol during 5 min in a microwave glass vessel. This was followed by addition of *N*-ethyldiisopropylamine (1 mL, 4.83 mmol) and methyl acrylate (3 mL, 0.047 mmol), and the mixture was sonicated during 2 min. Finally, a con- denser was placed and the mixture was irradiated at 60 °C working at 10 W for 60 min. After cooling at room tempera- ture, the crude was filtered on a Millipore membrane (GTTP, 0.2 1m) and washed by cycles of sonication and filtration using 75 mL of a mixture water/methanol (1:1). The collected black solid was finally dried under high vacuum affording 20 mg of *f*-CNH2.

### 2.3.2. Synthesis of gold dendrimer encapsulated nanoparticles (Au DENs)

Au nanoparticles encapsulated within fourth- and sixth-generation PAMAM dendrimers and containing 55 and 200 atoms, respectively were prepared according to previous reports [32,33].

### 2.3.3. Dendrimer-functionalized CNHs

*2.3.3.1. From f-CNH3 to f-CNH6.* Ten milligrams of *f*-CNH2 were suspended in 10 mL of methanol and sonicated for 10 min, followed by addition of the corresponding dendrimer: *f*-CNH3 (0.015 mL of PAMAM dendrimer G4-NH$_2$ (10 wt.% solution in methanol)), *f*-CNH4 (50 mL of PAMAM dendrimer G4-NH$_2$(Au$_{55}$) (1.6 1M) in water), *f*-CNH5 (0.13 mL of PAMAM dendrimer G6-NH$_2$ (5 wt.% solution in methanol)) and *f*-CNH6 (50 mL of G6-NH$_2$(Au$_{200}$) (1.6 1M) in water).

Then, a condenser was placed and the different reaction mixtures were heated at 40 °C for 1 day. Subsequently, the crudes were filtered on a Millipore membrane (GTTP, 0.2 1m) and washed by cycles of sonication and filtration using 75 mL of a mixture water/methanol (1:1). The collected black solids were finally dried under high vacuum affording 10 mg of *f*-CNH3, 10 mg of *f*-CNH4, 10 mg of *f*-CNH5 and 10 mg of *f*-CNH6, respectively.

### 2.4. Solubility measurements of hybrid CNH materials

One milligram of the sample was weighted and 0.1 mL of a solution composed of 2-[4-(2-hydroxyethyl)piperazin-1-yl] ethanesulfonic acid (HEPES), 10 mM (pH = 5.35) was added

followed by sonication for 5 min. This pH allows us to protonate the amino groups and to enhance the solubility of the system. The dispersion was checked visually. If the sample is not totally soluble, extra 0.1 mL of the solution was added followed by sonication (5 min). The sample was considered totally soluble when aggregates were not noticeable by the naked eye. The procedure was repeated until a clean dispersion was obtained and the solution kept stable for 24 h. This procedure renders the highest concentration possible for a fully dispersible sample and it gives us the corresponding solubility parameter.

### 2.5. Cell culture

The androgen-independent prostate cancer (PC-3) cells (kindly provided by Dr. P. Esbrit, Fundación Jiménez Díaz, Spain) were cultured in RPMI 1640 medium (Gibco, Invitrogen, Carlsbad, CA) supplemented with 10% Fetal Bovine Serum (FBS; Invitrogen), 2 mM L-glutamine (Invitrogen), 100 1g/mL streptomycin (Sigma, St. Louis, MO) and 100 IU/mL penicillin (Sigma). Cells were maintained in an incubator under a 5% CO$_2$ atmosphere at 37 °C.

### 2.6. Nanoparticle/siRNA interaction

Complexes between nanoparticles and siRNA were formed by mixing siRNA (100 nM) (Qiagen, Hilden, Germany) and nanoparticles at different nanoparticle nitrogen/siRNA phosphate (N/P) ratios, for 30 min at room temperature in diethylpyrocarbonate (DEPC) treated water. Then, cells at approximately 70–80% confluence were treated for 72 h, unless otherwise specified. Some experiments were carried out using a scramble (SCR) siRNA as mock control defining scramble siRNA as the one that does not encode for any mRNA. All experiments were carried out, at least, in triplicates.

### 2.7. Analysis of siRNA–nanoparticle complex formation and characterization

#### 2.7.1. Agarose gel retardation assay

Complexes between nanoparticles and siRNA were formed by mixing siRNA (100 nM) (Qiagen, Hilden, Germany) and nanoparticles at different nanoparticle nitrogen/siRNA phosphate (N/P) ratios, for 30 min at room temperature in DEPC-treated water. Complexes were, then analyzed by electrophoresis on a 1.2% agarose gel containing ethidium bromide. The binding capacity was evaluated based on the relative intensity of free siRNA band in each well referred to the intensity of siRNA alone [34].

#### 2.7.2. Polyanion competition assay

The ability of polyanions to displace siRNA from the nanoparticle was tested by exposing the nanoparticle/siRNA complex to increasing concentrations of the polyanion heparin (0, 0.5, 1, 1.5, and 3 1g/1g *f*-CNH3) as previously described [34]. Heparin, a polyanion capable of displacing polynucleotides from polycation/polynucleotide complexes, was chosen as a model substance for this assay, as previously reported by Merdan et al. [35]. This treatment resembles macromolecules that are present in the anionic environment of the cell cytosol.

*f*-CNH3/siRNA complexes were formed at N/P ratio of 3, to ensure complete binding of siRNA by the nanoparticle. The mixtures were run on an agarose gel as described above. The experiments were repeated three times with similar results.

### 2.7.3.  RNAse A protection assay

Protection of siRNA in the complexes against RNAse A digestion was investigated as previously reported [36]. Briefly, nanoparticle/siRNA complexes or naked siRNA (synonym of free siRNA, this means in the absence of any carrier) were prepared as previously described, and incubated with 0.25% RNAse A for 30 min at 37 °C. Then, RNAse A was inactivated and an excess of heparin was added to the samples to assure a complete siRNA release from the complex. Finally, samples were loaded on an agarose gel, in the same conditions as the experiments described above.

### 2.8.  siRNA uptake and toxicity

Uptakes of siRNA into PC-3 cancer cells and toxicity of the complexes were studied by flow cytometry using a fluorescein amidite-labeled siRNA (FAM-siRNA) and propidium iodide (PI). PI is not able to cross the cell membrane and therefore is generally excluded from viable cells. Because of this property, PI is commonly used for identifying dead cells in a population [37]. Briefly, complexes were prepared as described above. Cells were incubated with the FAM-labeled complexes or with naked FAM-siRNA for 72 h. PC-3 cells were then washed twice with cold (4 °C) phosphate-buffered saline (PBS, 150 mM NaCl; 10 mM sodium phosphate, pH 7.4) and incubated with 5 1g/mL propidium iodide (PI, Sigma) at 37 °C for 30 min in dark. After this, cells were analyzing using a flow cytometer (FACScalibur, 488 nm argon ion and 635 nm red diode lasers, Becton Dickinson, Oxford, UK). The percentage of positive cells was calculated [38] by setting the background population as 98% negative when analysing cells that had undergone transfection with FAM-siRNA alone. At least $10^4$ cells were analyzed for each condition. Data represent  mean + standard error of the mean (S.E.M.) of six experiments.

A similar study was performed using equivalent amounts of unaltered PAMAM dendrimers with respect to *f*-CNH3 sample.

### 2.9.  Real-time polymerase chain reaction (RT-PCR) analysis

Total cell RNA was isolated from cultured PC-3 cells using guanidine–phenol–chloroform thiocyanate following the manufacturer instructions (Tri-Reagent®, Sigma). The quality and concentration of RNA was quantified by spectrophotometry (Infinite 200, Tecan, Salzburg, Austria) using 1 1L of the RNA sample. Total RNA was always checked by running an aliquot in an agarose gel, to assess the integrity of the 18S and 28S mRNA bands. Cell total RNA (1–2 1g) was retrotranscribedusing a High Capacity cDNA Reverse Transcription Kit (Ap- plied Biosystems, Foster City, CA) according to the manufac-turer's instructions. The resulting cDNA was amplified using SYBR Green PCR Master mix (StepOne Real-Time PCR System; Applied Biosystems) and analyzed using commercial software (StepOne v2.0 software; Applied Biosystems). The specific primer pairs used for p42 MAPK were 5⁰-TTT-TGG-TTC-ATG-GCG-CTT-ACA-AGA-CTT-3⁰ (forward), 5⁰-TTT-GAA-TTC-ATT-TTA-ATC-CTG-CTT-3⁰ (reverse); and for GAPDH were 5⁰-ACCACAGTCCATGCCATCAC-3⁰ (forward), 5⁰-TCCAC-CACCCTGTTGCTGT-3⁰ (reverse). These sequences of primers had an annealing temperature of 60 °C. To confirm amplification specificity, the PCR products were subjected to a melting curve analysis. In order to guarantee the reliability of the results obtained, all samples were processed in triplicates. The quantification was performed by the comparative cycle threshold (Ct) method [39]. To normalize the data, the expression level of GAPDH RNA was used. Data represent mean ± - S.E.M. of four independent experiments run in triplicate each.

### 2.10.  Transfection efficiency assays

Fluorescent microscopy was used to provide direct evidence for the localization of the complexes and to assess the entrance of the siRNA/nanoparticle complexes within the PC-3 cells. Briefly, PC-3 cells were placed on glass cover-slips at a density of 4 · $10^4$ cells/dish. The FAM-siRNA/nanoparticle complexes were added to each dish and cells were then incubated at 37 °C. After 72 h, cells were washed with cold PBS. Images were acquired using a Nikon fluorescence microscope with the appropriate fluorescence filters (excitation wavelength of 490 nm and emission wavelength of 520 nm). Transfection efficiency was determined as the percentage of fluorescein-positive cells in nine randomly selected regions from three independent experiments.

### 2.11.  Cytotoxicity assays: 3-(4,5-dimethylthiazol-2-yl)-2,5-diphenyltetrazolium bromide (MTT) assay

The MTT method was selected to analyze detrimental intracellular effects on mitochondria and metabolic activity. The colorimetric MTT test, based on the selective ability of viable cells to reduce MTT to purple formazan, relies on intact metabolic activity and is frequently used for cytotoxicity screening [40]. The MTT cytotoxicity assay was performed as previously described [41]. Following 72 h incubation of PC-3 cells with the nanoparticle, MTT (5 mg/mL) was added to each well, being the volume of MTT added equal to one-tenth of the solution volume in the well and  the cells were incubated at 37 °C for 3 h. After this, culture medium was removed and the insoluble formazan crystals were dissolved in 250 1L DMSO (Sigma, Barcelona, Spain). The plate was agitated for 10 min and 200 1L from each well were then transferred to a 96-well microplate. The concentration of formazan was then determined spectrophotometrically (Infinite 200, Tecan) at540 nm with a reference filter at 685 nm. The data obtained represent mean + S.E.M. of three independent experimentsrun in quadruplicate each.

### 2.12.  Statistical analysis

All data are expressed as mean ± the standard error of the mean (S.E.M.) from at least three independent experiments. One-way analysis of variance (ANOVA) test followed by Bonferroni post hoc test was used to evaluate statistical differences between groups. $p < 0.05$ was considered statistically

## 3. Results and discussion

### 3.1. Synthesis and characterization of PAMAM–CNH systems

Pristine CNHs (*p*-CNHs) are not soluble in water or organic solvents and tend to aggregate as a result of strong van der Waals interactions. For biological applications functionalization of these nanostructures plays a fundamental role, enhancing solubility in aqueous media and providing a way to introduce new molecular entities with interesting properties.

Fig. 1 describes the synthetic methodology to achieve dendrimer attachment to the CNH surface. Firstly, we have followed a radical addition of Boc-protected substituted aniline in the presence of isoamyl nitrite as oxidizing agent, using water as the solvent [10]. This reaction was first described by Price and Tour [42] for the modification of carbon nanotubes and lately by our group using microwave activation [43,44]. Boc deprotection in acidic media is necessary to release the amino groups and use them as focal points to allow the subsequent reaction with methyl acrylate in basic conditions. It is worth to mention that this coupling was done under classical heating as well as under microwave irradiation (MW). While the functionalization is similar for both methods (data not shown for classical conditions), a reduction in time is clearly observed when microwave irradiation is used(3 days conventional heating [20,45] *vs.* 1 h under microwave irradiation). The double 1,4-Michael addition provides the ester groups necessary for the linkage with the PAMAM dendrimers.

Two different PAMAM dendrimers, in the absence and in the presence of gold nanoparticles, were attached to the CNHs: (i) fourth-generation PAMAM dendrimers, G4-NH$_2$ and G4-NH$_2$(Au$_{55}$), giving rise to *f*-CNH3 and *f*-CNH4, respectively. These dendrimers bear 64 primary amines on their surface and 62 inner tertiary amines; and (ii) sixth-generation PAMAM dendrimers, G6-NH$_2$ and G6-NH$_2$(Au$_{200}$), giving rise to *f*-CNH5 and *f*-CNH6, respectively. In these last dendrimers, there are 256 outer primary amines and 254 inner tertiary amines [46].

This synthetic methodology was chosen to avoid the aggregation of metal nanoparticles, because we have recently shown that the synthesis of Au DENs, followed by coupling to functionalized carbon nanomaterials is critical to achieve a good control of the size of Au particles [33].

Fig. 2 shows TEM images of different samples used in this work. In Fig. 2a, pristine CNHs are shown. Buds and dahlias are observed evidencing that the spherical aggregates are preserved after the functionalization. As dendrimers are not visible under the electron beam, no differences are noticed in the *f*-CNH aspect when compared with *p*-CNHs (Fig. S1). Fig. 2b and c illustrate representative TEM images of Au DENs deposited on the CNH surface. Histograms corresponding to these samples show sizes for Au particles that are bigger(2.0 ± 0.5 nm for G4-NH$_2$ and 2.8 ± 0.8 nm for G6-NH$_2$) when compared to the unaltered Au DENs (1.7 ± 0.4 and 2.0 ± 0.4 nm for G4-NH$_2$ and G6-NH$_2$ dendrimers, respectively, Fig. S2a–d). This result could be related to a visual overlap of the Au nanoparticles taking into account the three-dimensional structure of the CNH support and the limitation of the TEM that takes 2D images.

Fig. 2d shows a STEM–HAADF image of the Au DENs attached to CNHs. The high nuclear density of the Au particles
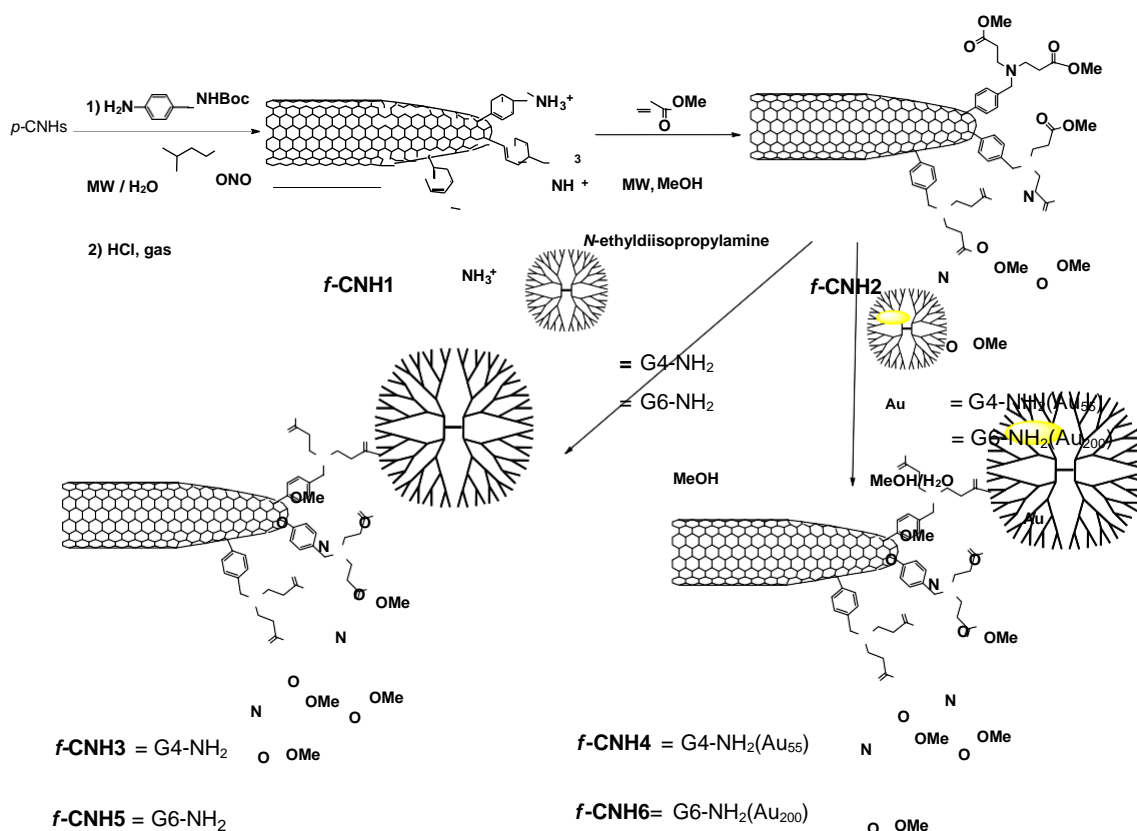
Fig. 1 – Synthesis of the dendrimer-functionalized carbon nanohorns. The symbol illustrated for the dendrimer represents fourth- and sixth-generation PAMAM dendrimers in the presence and in the absence of gold nanoparticles.
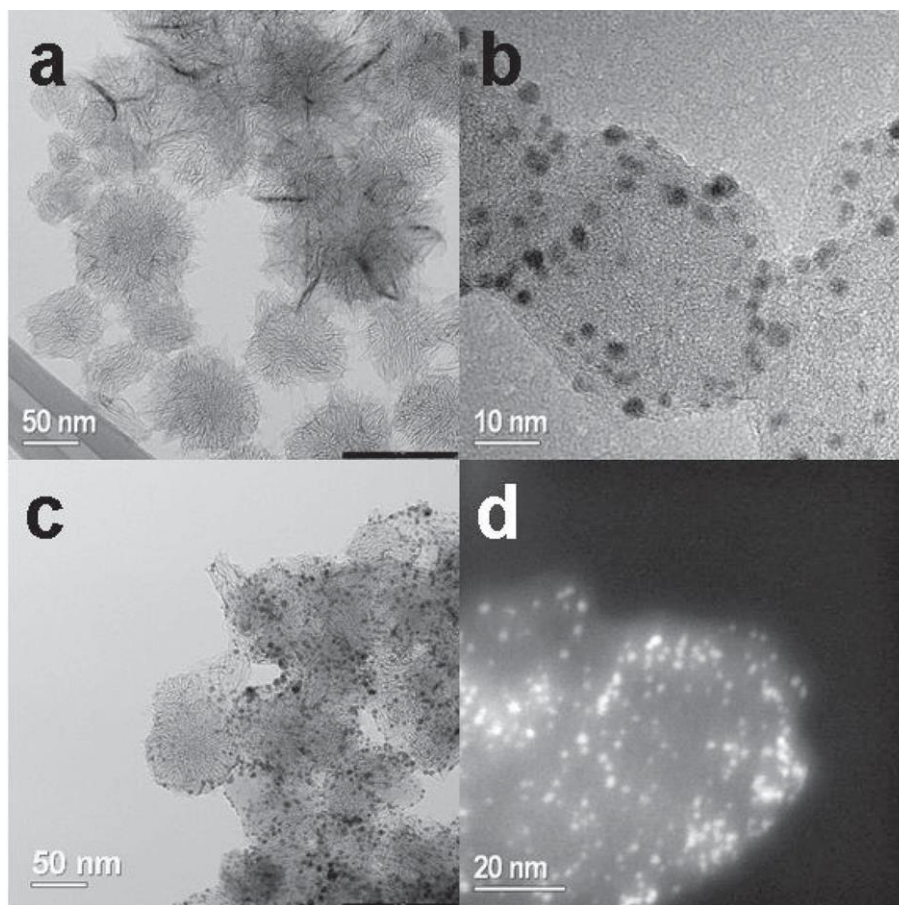
Fig. 2 – TEM images of (a) *p*-CNHs; (b) *f*-CNH4 and (c) *f*-CNH6. (d) Representative high-angular annular dark-field STEM image of *f*-CNH4.

| Table 1 – Size of the CNH derivatives determined through DLS technique. | | | | | | | |
|---|---|---|---|---|---|---|---|
| CNH sample | *p*-CNHs | 1 | 2 | 3 | 4 | 5 | 6 |
| DLS/nm | n.a.[a] | $62.5 \pm 4.4$ | $87.0 \pm 19.1$ | $78.0 \pm 14.8$[b] | $434.7 \pm 58.0$ | $70.3 \pm 12.6$ | $335.7 \pm 47.5$ |

[a] Data not available because of the lack of dispersability/solubility of the *p*-CNH in water.
[b] In this sample, two populations were noticed: 81% of aggregates show a hydrodynamic diameter of $78.0 \pm 14.8$ nm while the rest (19%) display a diameter that is $351.8 \pm 51.2$ nm (both populations contribute to the biological results displayed by *f*-CNH3 (see below).

provides good contrast of the metal along the surface of the CNHs [47]. In future studies, this will facilitate the recognition of the CNHs in the cellular media because cellular organelles have dimensions and electron contrast that are similar to CNHs. Au DENs are suitable as biological markers as Baker and co-workers have shown [48]. In this work, we use Au DENs as markers to determine the localization of the dendrimers along the surface of the carbon nanohorns. This is because each PAMAM dendrimer contains a single gold nanoparticle [28,49,50]. Although the amount of PAMAM dendrimers can be calculated by the use of other methods such as TGA, the presence of the Au particles allows the indirect visualization of the dendrimers.

TEM experiments prove that the functionalization does not influence the final CNH aggregate size, either dahlias or buds (Table S1). However, in order to know the aggregation
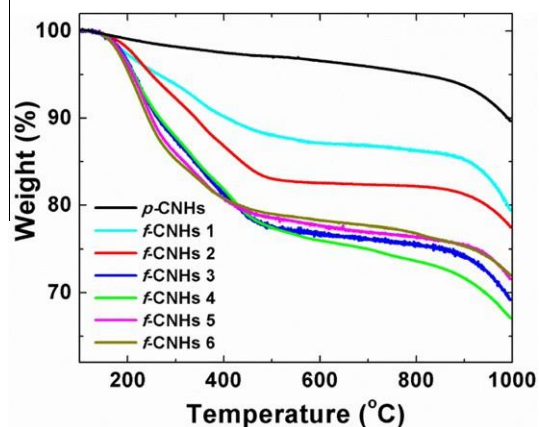


Fig. 3 – TGA of pristine and functionalized CNHs under $N_2$ atmosphere.

Table 2 – Functionalization data based on TGA results.

| Sample f-CNH | TGA (wt.% loss) | Functional group coverage[a] | 1mol Dendrimer/ g f-CNH[b] |
|---|---|---|---|
| 1 | 13 | 59 | – |
| 2 | 17 | 150 | – |
| 3 | 22 | 18,478 | 3.5 |
| 4 | 24 | 12,860 | 4.9 |
| 5 | 22 | 75,460 | 0.9 |
| 6 | 21 | 95,534 | 0.7 |

[a] Number of carbons of the CNH skeleton for every functional group added in each reaction (the number of attached functional groups was calculated based on the correspondent molecular weight and the weight loss at 550 °C. At this temperature PAMAM dendrimers are fully removed under nonoxidizing conditions and no decomposition of the p-CNHs is observed. Therefore, the measured weight loss from each sample at 550 °C can be attributed to loss of organic material. The residual mass was attributed to pristine CNHs, which was used to determine the mequiv of CNHs carbons present).

[b] Number of 1mol dendrimer attached per gram of f-CNH.
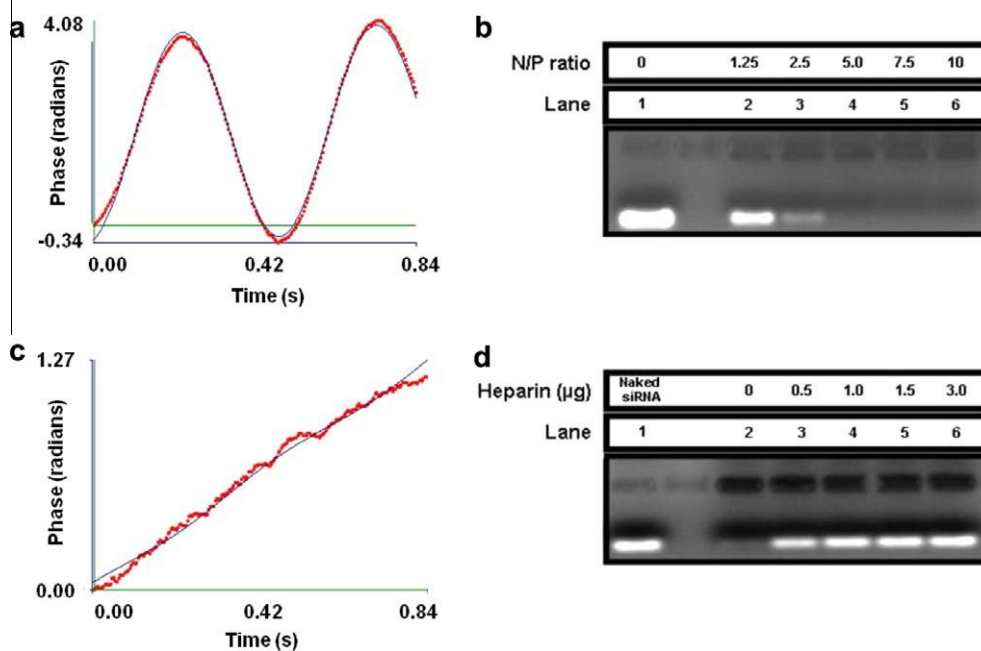


Fig. 4 – Interaction f-CNH3/siRNA. (a) Phase plot from a Z-potential measurement for f-CNH3 (8.3 1g/mL, pH = 5.35). (b) Gel electrophoresis shift assay at the indicated N/P ratios. (c) Phase plot from a Z-potential measurement for the complex f-CNH3/siRNA (8.3 1g/mL of f-CNH4 incubated with 33.3 nM of siRNA, pH = 5.35). (d) Polyanion displacement of nanoparticle-bound siRNA. f-CNH3/siRNA complexes were formed at N/P ratio of 3 and incubated with varying concentrations of Heparin (0, 0.5, 1, 1.5, and 3 1g/1g f-CNH3).

of these species in solution, photon correlation spectros-copy (PCS) experiments were performed. DLS techniques such as PCS are a common tool to study size distributions in situ. These studies allow the determination of the hydrodynamic diameter distribution of the dendrimer– nanoparticle ensemble. The hydrodynamic diameter is re- lated to the diffusion coefficient and can be calculated according to the Stokes–Einstein equation [51]. Considering that the average value obtained by TEM for dahlias and buds is 99 ± 14.4 and 45 ± 10.7 nm, respectively (Table S1),

and that values obtained using PCS gives an average be-tween these two CNH forms, the data obtained using this last technique for f-CNHs 1, 2, 3 and 5 are consistent with individual species or very small aggregates (Table 1). On the other hand, it is remarkable the strong aggregation that we notice when Au nanoparticles are hosted in the dendrimer cavities (f-CNHs 4 and 6). The presence of the Au nanocomposite could originate an aggregation process and these results are in agreement with a decrease in the solubility.

The amount of organic groups in the *f*-CNHs was determined by TGA.[1] Analysis of the weight loss allows us to know the number of 1mol of PAMAM dendrimer attached per gram of *f*-CNH. Fig. 3 shows the weight loss attributed to the attached organic materials onto the CNH surface. As a consequence, each reaction step has a lower yield than 100%. For instance, especially in the case of dendrimer attachment,the functional group coverage decreases quite a bit, but we have to consider that the dendrimer is spatially very demand-ing, so that it will cover several ester groups present in the surface. However, each step results in an increase of the molecular weight of these organic fragments and, thus, contributes to the addition of mass attached to the CNH surface (Table 2). The first step, namely the Tour reaction, shows a very high functionalization density, corresponding to about one functional group every 50 carbon atoms of the CNH surface. This result speaks about a very high concentration of functional groups, so that it will be less difficult to carry out the next steps. The highest weight loss values (∼22–24%) correspond to the dendrimer derivatives coupled to CNHs. When G4-NH$_2$ dendrimers are deposited on the CNHs we obtain a G4-NH$_2$ molecule per about 18,478 CNH carbons. This value is in the range of the corresponding one to G4-NH$_2$(Au$_{55}$) (12,860 CNH carbons/dendrimer). These data confirm that the gold nanoparticle hosted by the dendrimer does not affect the reactivity of the amine groups and the linkage to the ester moieties that are decorating the CNH surface. However, when G4-NH$_2$ values are compared with G6-NH$_2$ results, it is clear that the number of G6-NH$_2$ dendrimers deposited on the CNHs is much less than the corresponding to G4-NH$_2$. This is rationalized by the difference in size of the PAMAM dendrimers, G6-NH$_2$ has a bigger diameter than G4-NH$_2$ (6.7 *vs.* 4.5 nm, respectively) [46]. Therefore, we can conclude that the steric hindrance plays an important role in the incorpora- tion of dendrimers onto the CNH surface.

When an oxidizing atmosphere is used during the TGA, both functional groups and CNHs decomposed and the final mass residue at 800 °C reflects the amount of gold introduced in our carbon nanostructures (Fig. S3). The quantity of gold also allows us to corroborate the amount of dendrimers deposited on the CNHs. This is because each PAMAM dendrimer contains a single gold nanoparticle whose size will be related to the number of metal equivalents used in the synthesis of Au DENs [49]. Therefore, 1mol of Au nanoparti-cles should be similar to 1mol of PAMAM dendrimers. In the case of *f*-CNH4, the amount of gold in this sample is 7.4 1mol Au nanoparticle/g *f*-CNH while for *f*-CNH6, 2.5 1mol Au nanoparticle/g *f*-CNH were found.[2] These values are within the range of those obtained with TGA under nitrogen atmosphere (4.9 1mol dendrimer/g *f*-CNH for *f*-CNH4 and 0.7 1mol dendrimer/g *f*-CNH for *f*-CNH6).
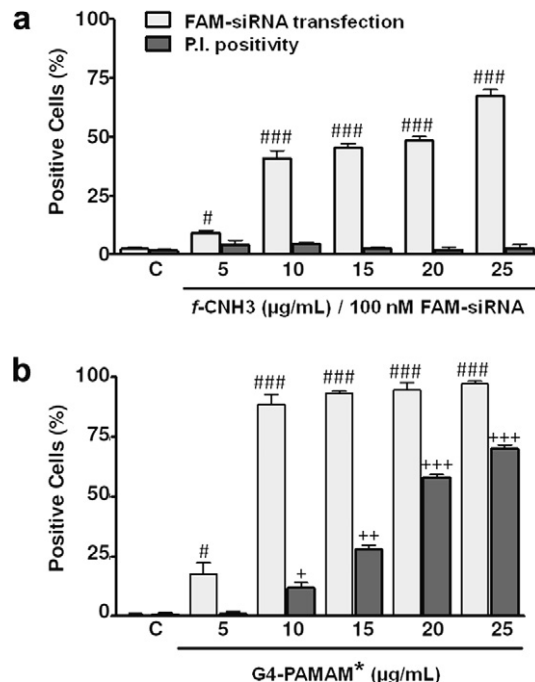


Fig. 5 – Simultaneous uptake and toxicity assays on PC-3 cells. (a) Increasing ratios of the complex *f*-CNH3/fluorescent siRNA were used to study uptake and toxicity with propidium iodide. (b) Similar study performed with unattached fourth-generation PAMAM dendrimers. *Calculated amounts of PAMAM dendrimers in 5–25 1g/mL of *f*-CNH3. Cells were analyzed by flow cytometry. #$p < 0.05$ and ###$p < 0.001$ as compared to naked siRNA (in the absence of any carrier) labeled with fluorescein amidite (FAM) treated control cells (C). +$p < 0.05$, ++$p < 0.01$ and +++$p < 0.001$ as compared to (C).

Pristine CNHs are not soluble in water. The introduction of functional groups enhances the solubility of CNHs, with the dendrimer derivatives displaying the higher dispersibility (Fig. S4). However, as previously mentioned, derivatives that contain gold nanoparticles are slightly less dispersible (*f*-CNH3 0.76 mg/mL *vs.* *f*-CNH4 0.47 mg/mL. See Section 2 for the procedure). It seems also that the dispersibility values depend more on the number of dendrimers attached to the CNHs than on the dendrimer dimensions or the number of positive charges in the derivatives. Thus, fourth-generation PAMAM derivative *f*-CNH3, that possesses a higher number of dendrimer units than the sixth-generation derivative*f*-CNH5 (Table 2), is the most soluble derivative (*f*-CNH3
0.76 mg/mL *vs.* *f*-CNH5, 0.57 mg/mL). This is supported by Z-potential values, which indicate a similar total number of positive charges for both derivatives (see Table S2).

---

[1] The number of attached functional groups was calculated based on the correspondent molecular weight and the weight loss at 550 °C. At this temperature PAMAM dendrimers are fully removed under non-oxidizing conditions and no decomposition of the *p*-CNHs is observed. Therefore, the measured weight loss from each sample at 550 °C can be attributed to loss of organic material. The residual mass was attributed to pristine CNHs, which was used to determine the mequiv of CNHs carbons present.

[2] The number of 1mol of Au DENs was calculated based on the correspondent molecular weight of a nanoparticle composed of 55 gold atoms for f-CNH4, 200 gold atoms for f-CNH6 and the weight loss at 800 °C. At this temperature all the organic fragments are fully removed and decomposition of the p-CNHs is observed. Therefore, the remaining weight from each sample at 800 °C can be attributed to gold particles.

## 3.2. Biological applications

As previously commented, these hybrid materials that combine carbon nanohorns and dendrimers are possible candidates for a wide-range of biological applications. Especially important is the suitability of the CNHs as ideal platforms where multiple drugs or vectors can be uploaded onto the carrier [52,53]. To this purpose, we have used the most soluble derivative synthesized in the present work. siRNA will bind electrostatically to the protonated amino groups located at the periphery of the PAMAM dendrimers at pH 5.35 (HEPES buffer, 0.01 M). We will consider that the total amount of primary amines are protonated at pH = 5.35 as these amines are more basic than the tertiary amines in PAMAM dendrimers [54,55].

Z-potential measurements give us an idea of the nature and the magnitude of the surface potential of our particles in solution. Our solution is placed under an electric field originated by two electrodes in a cuvette. Because of this electric field, the charged particles migrate and this movement originates the scattering of the incident laser. The phase is unaltered in the light scattered by the movement of the particles in solution, although is shifted in phase proportionally to their electrophoretic velocity. This phase shift is measured by comparing the phase of the light scattered by the particles with the phase of a reference beam. The Z-potential value is extremely related to the particles stability with respect to aggregation processes [56]. From this phase plot, a Z-potential value of $18.2 \pm 1.2$ mV (pH = 5.35, 10 mM HEPES solution) for $f$-CNH3 is obtained (Fig. 4a). This overall positive charge correlates well with the nature of $f$-CNH3 that holds numerous amino groups on the CNH surface (Table S2). The positive charges permit the dendriplex formation by electrostatic interaction with the phosphate groups of the nucleic acid. This process was studied by means of gel electrophoresis which will show a decrease in free dendrimer migrating through the electric field. Incubation of $f$-CNH3 with scram- bled siRNA (100 nM) shows that there is a complete binding of the siRNA at a nitrogen/siRNA phosphate (N/P) ratio of 5 (Fig. 4b). For the N/P calculation we have considered that only the outer primary amines of the PAMAM dendrimers are pro-tonated. The electrostatic binding that takes place between the genetic material and the $f$-CNH3 was also corroborated by Z-potential measurements. A negligible charge was deter- mined for the complex $f$-CNH3/siRNA ($0.2 \pm 0.2$ mV (pH = 5.35, 10 mM HEPES solution) Fig. 4c). This corroborates the full for- mation of the dendriplexes as these complexes have their charges neutralized. The binding between $f$-CNH3/siRNA was reversible and could be displaced by incubation with increasing concentrations of the polyanionic heparin achiev- ing a complete displacement in the presence of 1 lg of hepa- rin (Fig. 4d). Heparin would mimic the anionic groups in the cell cytosol providing an indication on whether the siRNA could be effectively released in the cells to exert its biological action. Also it provides information on the complex stability as well as its reversibility [34–36]. Moreover, siRNA bound to the hybrid material was protected from degradation by RNAseA (Fig. S5). These experiments allow us to conclude that $f$- CNH3 is able to bind siRNA and release it in the presence of polyanions (a treatment that resembles the cell cytosol). DLS experiments corresponding to the complex $f$-CNH3/siR- NA (8.3 lg/mL of $f$-CNH3 incubated with 33.3 nM of siRNA) run at pH = 5.35 did not show any appreciable change in the size of the dendriplex when compared to free $f$-CNH3 sample.
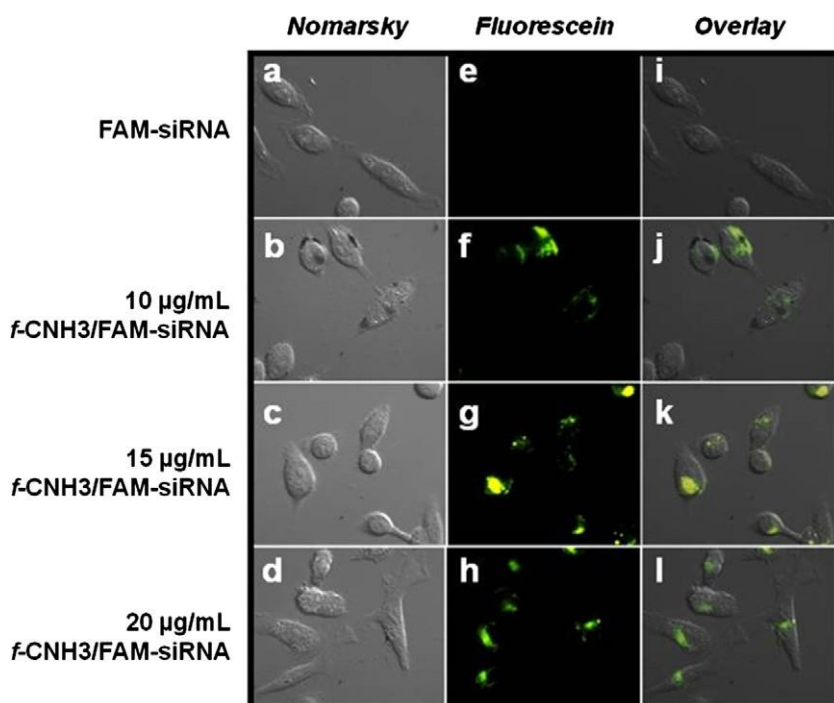


Fig. 6 – Fluorescence micrograph images of PC-3 cells treated for 72 h with naked FAM-siRNA (100 nM) (a and e) and FAM-siRNA (100 nM) complexed with $f$-CNH3 at 10 lg/mL (b and f), 15 lg/mL (c and g), or 20 lg/mL (d and h). The right column (i–l) represents the overlay of Nomarsky and fluorescein images.

Fig. 5a shows the transfection efficiency when using *f*-CNH3 as carrier while we also check the toxicity of the system at increasing concentrations of the complex *f*-CNH3/siRNA. For this purpose, PC-3 cells were incubated with the *f*-CNH3/fluorescein-labeled siRNA complexes for 72 h, followed by incubation with propidium iodide, a known marker of cell death (PI) [37]. Cells were analyzed for both fluorescein and propidium fluorescence by flow cytometry (see Section 2). As it can be observed in Fig. 5a, there is a concentration-dependent increase in the percentage of fluorescein-labeled cells. This indicates an increase in *f*-CNH3/siRNA complex internalization by the PC-3 cells. Moreover, it is interesting to note that there is not an increase in the number of propidium-labeled cells confirming the lack of cytotoxicity obtained by measuring MTT activity (Fig. S6). However, it is remarkable the cytotoxicity that similar amounts of free fourth-genera-tion PAMAM dendrimers display. This is shown in Fig. 5b, where increasing concentrations of the pristine dendrimers have as a consequence an increase in the toxicity measured with propidium iodide. The membrane disruption indicated with this experiment would also facilitate the entrance of
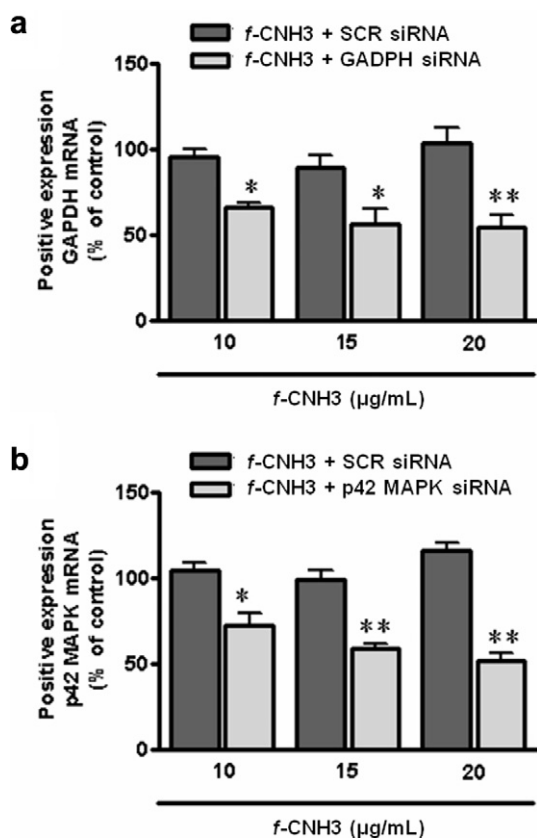
FAM-siRNA, increasing artifactually the number of fluorescein-positive cells. We can state that the complex formed by functionalized carbon nanohorns decorated with PAMAM dendrimers display less toxicity than unaltered dendrimers. *f*-CNH3 is safe to be employed at these concentrations. The lack of toxicity for these materials is in agreement with other reports where functionalized CNHs are applied in nanomedicine [2–4].

Fluorescence microscopy unequivocally demonstrates that only the siRNA (marked with a green fluorescent label) that is bound to *f*-CNH3 can enter PC-3 cells (Fig. 6) while naked siRNA is unable to cross the cell membrane as it is shown in Fig. 6e and i. These data are confirmed by means of flow cytometry (Fig. 5). Both techniques, fluorescence microscopy as well as flow cytometry are consistent and clearly show that an increase in the concentration of the hybrid nanomaterial up to 20 lg/mL results in higher incorporation of siRNA within the cells.

Incubation of a complex of increasing concentrations of *f*-CNH3 (10–20 lg/mL with GAPDH-specific siRNA (100 nM)) for 72 h resulted in a concentration-dependent reduction in GAPDH mRNA levels that reached about 50% inhibition at 20 lg/mL of *f*-CNH3 (Fig. 7a). No reduction in GAPDH mRNA levels was observed when PC-3 cells were incubated with naked siRNA (in the absence of carrier, data not shown), or with the complex *f*-CNH3/scramble siRNA. This suggests a specific effect that takes place when a specific siRNA is transported into the cell by the nanohybrid *f*-CNH3. The ability shown by *f*-CNH3 to decrease the house-keeping GAPDH mRNA levels indicates that the siRNA escapes the endosome/lysosome and is able to bind to mRNA [57]. A similar effect was ob- served using a siRNA specific for p42-MAPK (Fig. 7b) decreas-ing the mRNA levels of this protein. The protein p42-MAPK belongs to the MAPK cascade that is related to many mecha- nisms involved in cancer such as proliferation, apoptosis and survival [58]. Remarkably, when similar amounts of free fourth-generation PAMAM dendrimers to those present in Fig. 7 are used in similar transfection assays (Fig. S7), no reduction is noticed for a concentration of dendrimers that corresponds to 10 lg/mL of *f*-CNH3. In case of higher concen-trations, an important reduction in the mRNA levels is ob- served. However, at those concentrations, free fourth- generation PAMAM dendrimers are clearly cytotoxic as the MTT experiments (Fig. S6) and propidium iodide toxicity mea-surements (Fig. 5b) demonstrate.

This information allows us to conclude that *f*-CNH3/siRNA complexes decrease mRNA levels in PC-3 cells without cyto-toxicity up to 25 lg/mL suggesting that this non-viral vector might have a role to deliver siRNA to cancer cells.



Fig. 7 – Transfection assay for *f*-CNH3. PC-3 cells exposed for 72 h to different amounts of *f*-CNH3 complexed with scramble (SCR) or specific siRNA (100 nM) and the levels of mRNA encoding for (a) the house keeping protein GAPDH or (b) the p42 mitogen-activated protein kinase (p42-MAPK) were determined using quantitative RT-PCR. Non-treated PC-3 cells were used as the control (100% of the signal). $^*p < 0.05$; $^{**}p < 0.01$ as compared to control untreated cells. Scramble siRNA does not encode for any mRNA and it is used as a mock control as indicated in Section 2.

## 4.    Conclusions

A new series of hybrid materials composed of carbon nano-horns as support and different PAMAM dendrimers as siRNA graspers have been synthesized and fully characterized. The introduction of multiple functional groups in different steps has contributed to an enhancement of the CNH water solubility, especially the final introduction of the PAMAM den-drimers with several amino groups leads to more soluble CNHs and therefore biologically compatible. This biological

compatibility is mainly driven by the high carbon surface area that originates awell-distributed positive charge when PAMAM dendrimers are attached. The ability of PAMAM dendrimers to host Au nanoparticles (1–2 nm) has been used to determine the localization of the dendrimers on the CNH surface. Proof of concept on the transfection efficiency of the most promising hybrid among the new synthesized compounds is also presented. This hybrid, which is made of fourth-generation PAMAM dendrimers and CNHs, does not display any cytotoxicity up to 25 1g/mL while it is very effective to couple siRNA. In fact, similar concentrations of unaltered PAMAM dendrimers show toxicity as proved with propidium iodide experiments. The biological data are promising for these non-viral vectors with emphasis in the fact that the complex composed of *f*-CNH3 and the specific siRNA is able to diminish the house-keeping GAPDH mRNA levels as well as the mRNA levels of the protein p42 mitogen-activated protein kinase (p42-MAPK), protein directly involved in cancer development.

The importance of these novel hybrid nanocomposites based on CNHs and PAMAM dendrimers relies on two aspects: (a) its lower toxicity than the individual carbon nanoparticle or dendrimers which make them more suitable for biological applications; and (b) the ''proof of concept'' that these new hybrids are able to transfect efficiently siRNA, allowing their structure further chemical modifications to improve transfection efficiency in different cell types.

The aforementioned properties would improve the hybrid biodistribution and biocompatibility that are the two key issues that need to be overcome before nanoparticles turn to be routine for gene therapy [53]. Current works are being developed in our laboratories to improve the gene delivery efficiency of these systems.

## Acknowledgments

REFERENCES

[1] Iijima S, Yudasaka M, Yamada R, Bandow S, Suenaga K, Kokai F, et al. Nano-aggregates of single-walled graphitic carbon nano-horns. Chem Phys Lett 1999;309(3–4):165–70.

[2] Miyawaki J, Yudasaka M, Azami T, Kubo Y, Iijima S. Toxicity of single-walled carbon nanohorns. ACS Nano 2008;2(2):213–26.

[3] Lynch RM, Voy BH, Glass DF, Mahurin SM, Zhao B, Hu H, et al. Assessing the pulmonary toxicity of single-walled carbon nanohorns. Nanotoxicology 2007;1(2):157–66.

[4] Fan X, Tan J, Zhang G, Zhang F. Isolation of carbon nanohorn assemblies and their potential for intracellular delivery. Nanotechnology 2007;18:195103–9.

[5] Ajima K, Yudasaka M, Murakami T, Maigne A, Shiba K, Iijima S. Carbon nanohorns as anticancer drug carriers. Mol Pharm 2005;2(6):475–80.

[6] Ajima K, Murakami T, Mizoguchi Y, Tsuchida K, Ichihashi T, Iijima S, et al. Enhancement of in vivo anticancer effects of cisplatin by incorporation inside single-wall carbon nanohorns. ACS Nano 2008;2(10):2057–64.

[7] Murakami T, Fan J, Yudasaka M, Iijima S, Shiba K. Solubilization of single-wall carbon nanohorns using a PEG–doxorubicin conjugate. Mol Pharm 2006;3(4):407–14.

[8] Murakami T, Ajima K, Miyawaki J, Yudasaka M, Iijima S, Shiba K. Drug-loaded carbon nanohorns: adsorption and release of dexamethasone in vitro. Mol Pharm 2004;1(6):399–405.

[9] Miyawaki J, Yudasaka M, Imai H, Yorimitsu H, Isobe H, Nakamura E, et al. In vivo magnetic resonance imaging of single-walled carbon nanohorns by labeling with magnetite nanoparticles. Adv Mater 2006;18(8):1010–4.

[10] Rubio N, Herrero MA, Meneghetti M, Dı´az-Ortiz A, Schiavon M, Prato M, et al. Efficient functionalization of carbon nanohorns via microwave irradiation. J Mater Chem 2009;19:4407–13.

[11] Isobe H, Tanaka T, Maeda R, Noiri E, Solin N, Yudasaka M, et al. Preparation, purification, characterization, and cytotoxicity assessment of water-soluble, transition-metal-free carbon nanotube aggregates. Angew Chem Int Ed 2006;45(40):6676–80.

[12] Pagona G, Karousis N, Tagmatarchis N. Aryl diazonium functionalization of carbon nanohorns. Carbon 2008;46(4):604–10.

[13] Vashist SK, Zheng D, Pastorin G, Al-Rubeaan K, Luong JHT, Sheu FS. Delivery of drugs and biomolecules using carbon nanotubes. Carbon 2011;49(13):4077–97.

[14] Shi X, Wang SH, Shen M, Antwerp ME, Chen X, Li C, et al. Multifunctional dendrimer-modified multiwalled carbon nanotubes: synthesis, characterization, and in vitro cancer cell targeting and imaging. Biomacromolecules 2009;10(7):1744–50.

[15] Lacerda L, Bianco A, Prato M, Kostarelos K. Carbon nanotube cell translocation and delivery of nucleic acids in vitro and in vivo. J Mater Chem 2008;18(1):17–22.

[16] Podesta JE, Al-Jamal KT, Herrero MA, Tian B, Ali-Boucetta H, Hegde V, et al. Antitumor activity and prolonged survival by carbon-nanotube-mediated therapeutic siRNA silencing in a human lung xenograft model. Small 2009;5(10):1176–85.

[17] Lacerda L, Soundararajan A, Singh R, Pastorin G, Al-Jamal K, Turton J, et al. Dynamic imaging of functionalized multi-walled carbon nanotube systemic circulation and urinary excretion. Adv Mater 2008;20(2):225–30.

[18] Lacerda L, Ali-Boucetta H, Herrero MA, Pastorin G, Bianco A, Prato M, et al. Tissue histology and physiology following intravenous administration of different types of functionalized multiwalled carbon nanotubes. Nanomedicine-UK 2008;3:149–61.

[19] Al-Jamal KT, Gherardini L, Bardi G, Nunes A, Guo C, Bussy C, et al. Functional motor recovery from brain ischemic insult by carbon nanotube-mediated siRNA silencing. Proc Natl Acad Sci USA 2011;108:10952–5720.

[20] Herrero MA, Toma FM, Al-Jamal KT, Kostarelos K, Bianco A, Da Ros T, et al. Synthesis and characterization of a carbon nanotube–dendron series for efficient siRNA delivery. J Am Chem Soc 2009;131(28):9843–8.

[21] Pan BF, Cui DX, Xu P, Chen H, Liu FT, Li Q, et al. Design of dendrimer modified carbon nanotubes for gene delivery. Chin J Cancer Res 2007;19(1):1–6.

[22] Al-Jamal KT, Toma FM, Yilmazer A, Ali-Boucetta H, Nunes A, Herrero MA, et al. Enhanced cellular internalization and gene silencing with a series of cationic dendron-multiwalled carbon nanotube:siRNA complexes. FASEB J 2010;24(11):4354–65.

[23] Zhang M, Yudasaka M, Ajima K, Miyawaki J, Iijima S. Light-assisted oxidation of single-wall carbon nanohorns for abundant creation of oxygenated groups that enable chemical modifications with proteins to enhance biocompatibility. ACS Nano 2007;1(4):265–72.

[24] Boas U, Christensen JB, Heegaard PMH. Dendrimers in medicine and biotechnology. New molecular tools. RSC Publishing; 2006. p. 62–85.

[25] Sonawane ND, Szoka Jr FC, Verkman AS. Chloride accumulation and swelling in endosomes enhances DNA transfer by polyamine–DNA polyplexes. J Biol Chem 2003;278:44826–31.

[26] Dobrovolskaia MA, McNeil SE. Immunological properties of engineered nanomaterials. Nat Nano 2007;2(8):469–78.

[27] Wiethoff CM, Middaugh CR. Barriers to nonviral gene delivery. J Pharm Sci 2003;92(2):203–17.

[28] Myers VS, Weir MG, Carino EV, Yancey DF, Pande S, Crooks RM. Dendrimer-encapsulated nanoparticles: new synthetic and characterization methods and catalytic applications. Chem Sci 2011;2(9):1632–46.

[29] Schiavon M, inventor. Device and method for production of carbon nanotubes, fullerene and their derivatives. Europe patent EP1428794 (A2); 2004 June 16.

[30] Schiavon M, inventor. Device and method for production of carbon nanotubes, fullerene and their derivatives.US2004213727 (A1); 2004 October 28.

[31] Morrison ID, Grabowski EF, Herb CA. Improved techniques for particle size determination by quasi-elastic light scattering. Langmuir 1985;1(4):496–501.

[32] Kim Y-G, Oh S-K, Crooks RM. Preparation and characterization of 1–2 nm dendrimer-encapsulated gold nanoparticles having very narrow size distributions. Chem Mater 2004;16:167–72.

[33] Herrero MA, Guerra J, Myers VS, Gomez MV, Crooks RM, Prato M. Gold dendrimer-encapsulated nanoparticles as labeling agents for multi-walled carbon nanotubes. ACS Nano 2010;4:905–12.

[34] Xiong XB, Uludag H, Lavasanifar A. Biodegradable amphiphilic poly(ethylene oxide)–block-polyesters with grafted polyamines as supramolecular nanocarriers for efficient siRNA delivery. Biomaterials 2009;30(2):242–53.

[35] Merdan T, Callahan J, Petersen H, Kunath K, Bakowsky U, Kopeckova P, et al. Pegylated polyethylenimine-Fab' antibody fragment conjugates for targeted gene delivery to human ovarian carcinoma cells. Bioconjugate Chem 2003;14(5):989–96.

[36] Rodrigo AC, Rivilla I, Pérez-Martínez FC, Monteagudo S, Ocaña V, Guerra J, et al. Efficient, non-toxic hybrid PPV–PAMAM dendrimer as a gene carrier for neuronal cells. Biomacromolecules 2011;12(4):1205–13.

[37] Moore A, Donahue CJ, Bauer KD, Mather JP. Simultaneous measurement of cell cycle and apoptotic cell death. In: Jennie PMaD, editor. Methods in cell biology. Animal cell culture methods, vol. 57. Academic Press; 1998. p. 265–78.

[38] Lampariello F. Evaluation of the number of positive cells from flow cytometric immunoassays by mathematical modeling of cellular autofluorescence. Cytometry 1994;15(4):294–301.

[39] Livak KJ, Schmittgen TD. Analysis of relative gene expression data using real-time quantitative PCR and the 2(-Delta Delta C(T)) Method. Methods 2001;25(4):402–8.

[40] Bermejo JF, Ortega P, Chonco L, Eritja R, Samaniego R, Mũllner M, et al. Water-soluble carbosilane dendrimers: synthesis biocompatibility and complexation with oligonucleotides; evaluation for medical applications. Chem Eur J 2007;13(2):483–95.

[41] Posadas I, Lopez-Hernandez B, Clemente MI, Jimenez JL, Ortega P, De la Mata J, et al. Highly efficient transfection of rat cortical neurons using carbosilane dendrimers unveils a neuroprotective role for HIF-1 alpha in early chemical hypoxia-mediated neurotoxicity. Pharm Res 2009;26(5):1181–91.

[42] Price BK, Tour JM. Functionalization of single-walled carbon nanotubes ''On Water''. J Am Chem Soc 2006;128(39):12899–904.

[43] Brunetti FG, Herrero MA, de Muñoz J, Díaz-Ortiz A, Alfonsi J, Meneghetti M, et al. Microwave-induced multiple functionalization of carbon nanotubes. J Am Chem Soc 2008;130(25):8094–100.

[44] Rubio N, Herrero MA, de la Hoz A, Meneghetti M, Prato M, Vázquez E. Versatile microwave-induced reactions for the multiple functionalization of carbon nanotubes. Org Biomol Chem 2010;8:1936–42.

[45] Campidelli S, Sooambar C, Lozano Diz E, Ehli C, Guldi DM, Prato M. Dendrimer-functionalized single-wall carbon nanotubes: synthesis, characterization, and photoinduced electron transfer. J Am Chem Soc 2006;128(38):12544–52.

[46] Tomalia DA, Baker H, Dewald J, Hall M, Kallos G, Martin S, et al. A new class of polymers: starburst-dendritic macromolecules. Polym J 1985;17(1):117–32.

[47] Garcia-Gutierrez D, Gutierrez-Wing C, Miki-Yoshida M, Jose-Yacaman M. HAADF study of Au–Pt core–shell bimetallic nanoparticles. Appl Phys A 2004;79(3):481–7.

[48] Shukla R, Hill E, Shi X, Kim J, Muniz MC, Sun K, et al. Tumor microvasculature targeting with dendrimer-entrapped gold nanoparticles. Soft Matter 2008;4:2160–3.

[49] Scott RWJ, Wilson OM, Crooks RM. Synthesis, characterization and applications of dendrimer-encapsulated nanoparticles. J Phys Chem B 2005;109:692–704.

[50] Gomez MV, Guerra J, Velders AH, Crooks RM. NMR characterization of fourth-generation PAMAM dendrimers in the presence and absence of palladium dendrimer-encapsulated nanoparticles. J Am Chem Soc 2009;131(1):341–50.

[51] Pecora R. Dynamic light scattering measurement of nanometer particles in liquids. J Nanopart Res 2000;2(2):123–31.

[52] Posadas I, Guerra J, Ceña V. Non-viral vectors for the delivery of siRNA to the central nervous system. Nanomedicine-UK 2010;5(8):1219–36.

[53] Pérez-Martínez FC, Posadas I, Guerra J, Ceña V. Barriers to non-viral vectors-mediated gene delivery in the nervous system. Pharm Res 2011;28(8):1843–58.

[54] Niu Y, Sun L, Crooks RM. Determination of the intrinsic proton binding constants for poly(amidoamine) dendrimers via potentiometric pH titration. Macromolecules 2003;36(15):5725–31.

[55] Cakara D, Kleimann J, Borkovec M. Microscopic protonation equilibria of poly(amidoamine) dendrimers from macroscopic titrations. Macromolecules 2003;36(11): 4201–4207.

[56] Kim T, Lee K, Gong MS, Joo SW. Control of gold nanoparticle aggregates by manipulation of interparticle interaction. Langmuir 2005;21(21):9524–8.

[57] Curtis CD, Nardulli AM. Using RNA interference to study protein function. The nuclear receptor superfamily. 505 ed.; 2009. p. 187–204.

[58] Koul HK, Maroni PD, Meacham RB, Crawford D, Koul S. p42/p44 Mitogen-activated protein kinase signal transduction pathway: a novel target for the treatment of hormone-resistant prostate cancer? Ann NY Acad Sci 2004;1030(1):243–52.

**Carbon nanohorns functionalized with polyamidoamine dendrimers as efficient biocarrier materials for gene therapy.**

*Javier Guerra, M. Antonia Herrero, Blanca Carrión, Francisco C. Pérez-Martínez, Maribel Lucío, Noelia Rubio, Moreno Meneghetti, Maurizio Prato, Valentín Ceña, Ester Vázquez\**
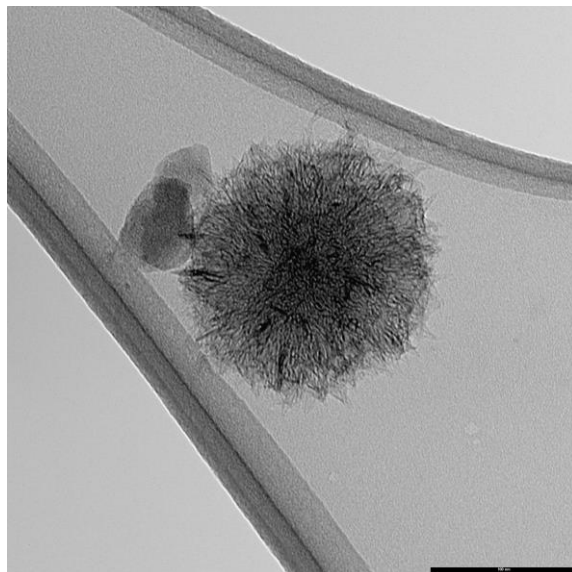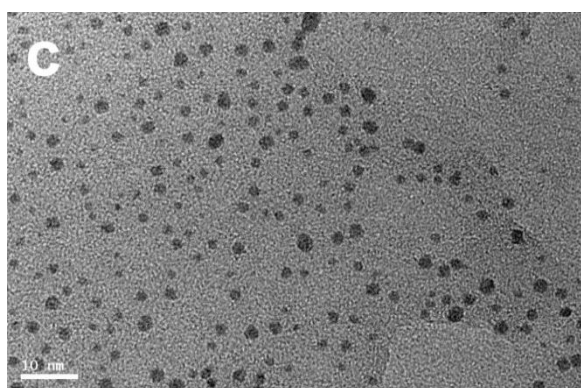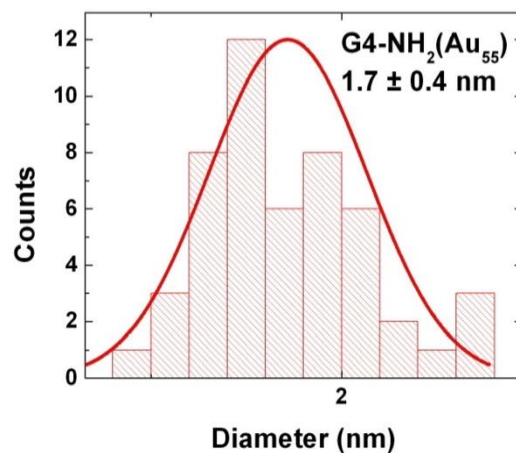
**Figure S1.** Representative TEM image of *f*-**CNHs 3** deposited on a lacey carbon grid. Black scale bar represents 100 nm.
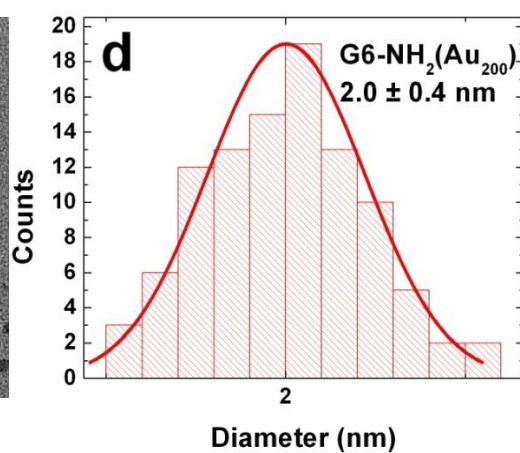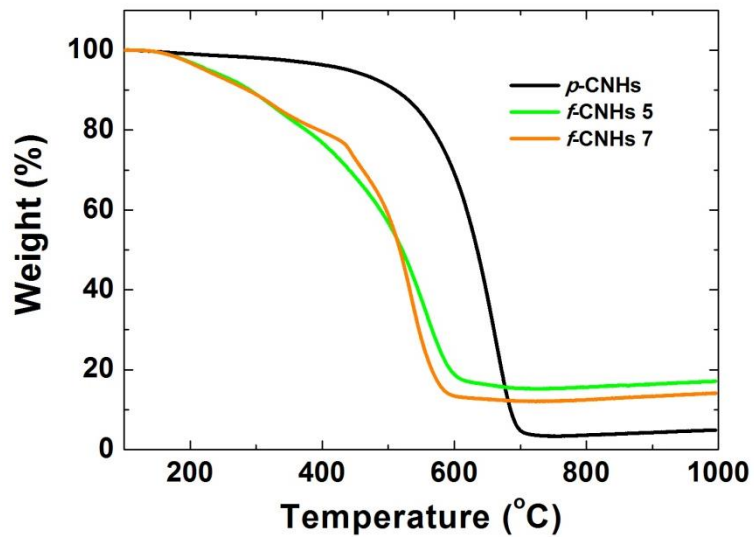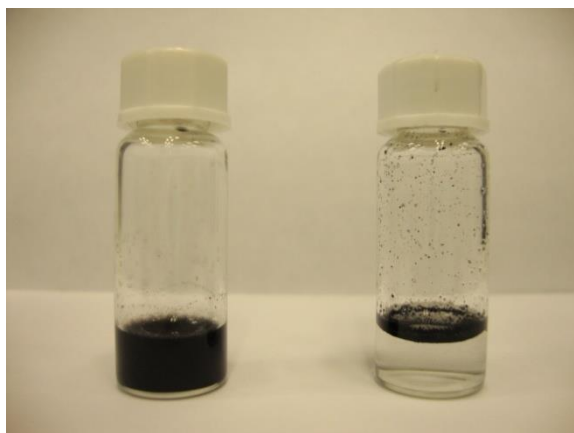
**Guerra, J. et al./Figure S1**
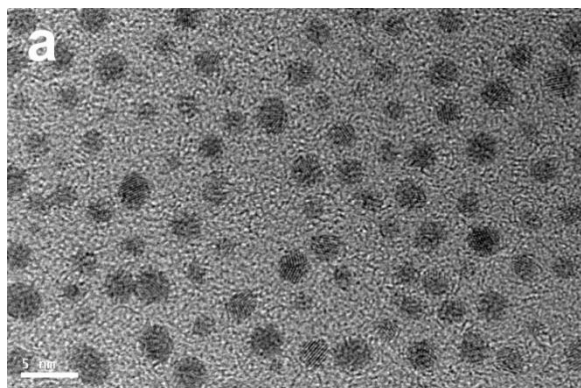
**Figure S2.** (a) TEM image of G4-NH$_2$(Au$_{55}$); (b) histogram of the previous sample; (c) TEM image of G6-NH2(Au$_{200}$) and (d) histogram of the previous sample.

**Guerra, J. et al./Figure S2**

**Figure S3.** TGA of pristine and functionalized CNHs bearing Au DENs under an oxidizing atmosphere.

**Figure S4.** Optical micrograph of vials containing aqueous solutions of *f*-**CNH3** (0.76 mg/mL) (left) and *p*-**CNHs** (1 mg/mL) (right).

**Figure S5.** *f*-**CNH3** protects siRNA against RNAse A. siRNA was complexed with *f*-**CNH3** as indicated in the Experimental Section. When indicated, the mixture was incubated in the presence of 0.25 % RNAse A. After RNAse A inactivation, siRNA was released from the complex by exposure to heparin (one µg). The experiment was repeated 3 times with similar results.

**Lane 1:** free siRNA band is observed and it is used as control.

**Lane 2:** the absence of the free siRNA band indicates the degradation because of the RNAse A action.

**Lane 3:** the absence of the free siRNA band indicates the complexation of the polynucleotide with the hybrid carrier *f*-**CNH3.**

**Lane 4:** the presence of the siRNA band confirms the release of the siRNA and the reversibility of the siRNA/nanoparticle complex formation.

**Lane 5:** the presence of the siRNA band indicates the successful protection of the siRNA performed by the nanoparticle *f*-**CNH3** in the presence of RNAse A that has not been able to degrade the siRNA. After treatment with RNAse A, the complex was put in the presence of heparin to observe the successful release of unaltered siRNA.

<div align="right">

**Guerra, J. et al./Figure S5**

</div>
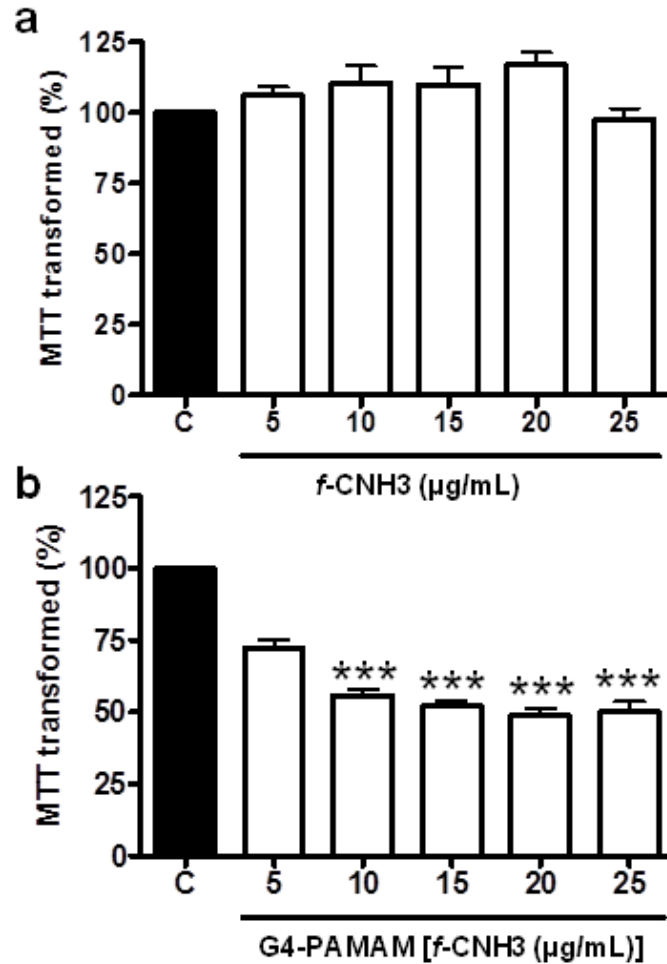
**Figure S6.** (a) Cytotoxicity of *f*-CNH3 on prostate cancer cells. (b) Cytotoxicity of fourth-generation PAMAM dendrimers on prostate cancer cells. Equivalent amounts of dendrimers to those present in each experiment in the Figure S6a are used. Cells were treated with increasing concentrations of *f*-CNH3 for 72 h and the cellular viability was assayed by measuring: (a) The percentage of 3-(4,5-Dimethylthiazol-2-yl)-2,5-diphenyltetrazolium bromide (MTT) transformed related to that in control (untreated) cells. ***$p < 0.001$ as compared to control cells (C).

Figure S6 demonstrates that *f*-CNH3 lacks toxicity on PC-3 cells. Incubation of PC-3 cells with increasing concentrations of *f*-CNH3 ranging from 5 to 25 µg/mL did not show any increase in toxicity when measured by determining the activity of either MTT (Figure S6a). However, when equivalent

amounts of unaltered G4-PAMAM dendrimers with respect to Figure S6a are used, clear cytotoxicity is observed for all the concentrations.

In other terms, similar amount of PAMAM dendrimers are more toxic when they are free (Figure S6b) than when they are anchored on the CNH surface (Figure S6a).

**Guerra, J. et al./Figure S6**
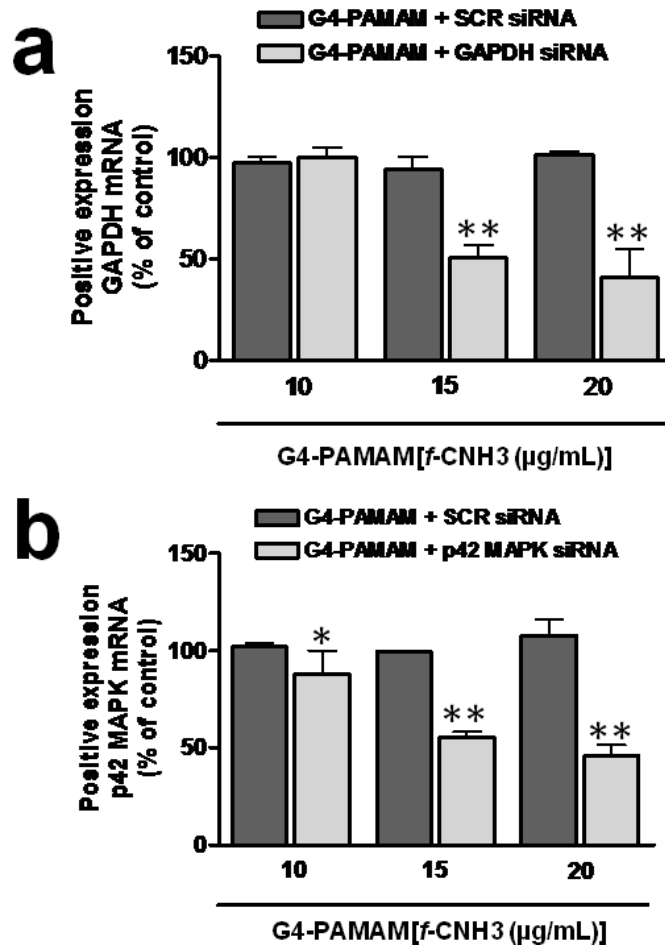
**Figure S7.** Transfection assay for free PAMAM dendrimers. PC-3 cells exposed for 72h to equivalent amounts of dendrimers to those present in each experiment in the Figure 7 complexed with scramble (SCR) or specific siRNA (100 nM) and the levels of mRNA encoding for a) the house keeping protein GAPDH or b) the p42 Mitogen-Activated Protein Kinase (p42-MAPK) were determined using Quantitative RT-PCR. Non-treated PC-3 cells were used as the control (100% of the signal). *p< 0.05; **p< 0.01 as compared to control untreated cells. Scramble siRNA does not encode for any mRNA and it is used as a mock control as indicated in the experimental section.

When similar amounts of free fourth-generation PAMAM dendrimers to those present in Figure 7 are used in similar transfection assays, no reduction is noticed for a concentration of dendrimers that

corresponds to 10 µg/mL of *f*-**CNH3**. In case of higher concentrations, an important reduction in the mRNA levels is observed. However, at those concentrations, free fourth-generation PAMAM dendrimers are clearly cytotoxic as the MTT experiments (Figure S6) and propidium iodide toxicity measurements (Figure 5) demonstrate.

**Guerra, J. et al./Figure S7**

**Table S1.** Size of CNH dahlias and buds determined by means of TEM.

| CNH sample | *p*-CNHs | 1 | 3 | 4 | 5 | 6 |
|---|---|---|---|---|---|---|
| TEM dahlia /nm | 99.7± 14.4 (20) | 100.7± 14.2 (4) | 92.0± 39.6 (8) | 94.7± 5.0 (5) | 78.9 (1) | n.a.[a] |
| TEM bud /nm | 45.0± 10.7 (73) | 42.4± 10.7 (23) | 35.0± 10.4 (48) | 47.9± 6.3 (18) | 41.2± 8.9 (23) | 33.9± 5.2 (8) |

Values between brackets indicate the number of structures measured. [a]Data not available because of the absence of individual dahlias in the grids.

**Guerra, J. et al./Table S1**

**Table S2.** Z-potential values in solutions containing 10 mM HEPES (pH = 5.35)

| CNH sample | *f*-CNHs 3 | *f*-CNHs 4 | *f*-CNHs 5 | *f*-CNHs 6 |
|---|---|---|---|---|
| Charge /mV | 18.2±1.2 | 8.4±2.7 | 16.6±2.6 | 11.9±2.2 |

**Guerra, J. et al./Table S2**